Abstract

Mass consistent models have been widely use in three-dimensional wind modelling by finite element method. In general, these problems are defined over regions with complex terrain and variable roughness length, therefore a suitable discretization of the studied zone will be necessary. In addition, there often exist points where more accuracy is required. We have used a method for constructing tetrahedral meshes which are simultaneously adapted to the terrain orography and the roughness length by using a refinement/derefinement process in a 2-D mesh corresponding to the terrain surface, following the technique proposed in [1, 2, 3]. In this 2-D mesh we include a local refinement around several points which are previously defined by the user. Besides, we develop a technique for adapting the mesh to any contour that has an important role in the simulation, like shorelines or roughness length contours [4, 5]. The final tetrahedral mesh is also constructed with more density of nodes near the terrain. The regions where more density of points is needed for obtaining a more accurate solution, are locally refined with the procedure proposed in [6].

This wind model improves that proposed in [7, 8]. The characterization of the atmospheric stability is carried out by means of the experimental measures of the intensities of turbulence. On the other hand, since several measures are often available at a same vertical line, we have constructed a least square optimization of such measures for developing a vertical profile of wind velocities from an optimum friction velocity.

The three main parameters governing the model are estimated using genetic algorithms with a parallel implementation [8, 9, 10]. For a given episode, we periodically update these parameters.

In order to test the model, some numerical experiments are presented, comparing the results with realistic measures.

1 Introduction

The society has been becoming aware of environmental problems and nowadays it appreciates the use of renewable energies. Along last years the use of wind power for producing electric energy has augmented considerably. So companies of this sector are requesting more and more sophisticated tools which allow them to face the competitive and demanding market. Wind models are tools that allow the study of several problems related to the atmosphere, such as, the effect of wind on structures, pollutant transport, fire spreading, wind farm location, etc.

Diagnostic models are not used to make forecasts through integrating conservative relations [11]. Therefore they are also called kinetic models [12]. This models generate wind fields that satisfy some physical conditions. If mass conservation law is the only imposed equation, we are defining a mass consistent model. The relative simplicity of diagnostic models makes them attractive from the practical point of view, since they do not require many input data and may be easily used. Pennel et al [13] checked that, in some cases, improved mass consistent models such as NOABL and COMPLEX obtained better results than other dynamic models which are more complex and expensive. However, we have to take into account that diagnostic models neither consider thermal effects nor those due to pressure gradients. As a consequence, problems like sea breezes can not be simulated with these models unless such effects are incorporated into the initial wind data using observations made in selected locations [14, 15]. So diagnostic models have been designed for predicting the effects of the orography on the steady average wind, i.e., average wind in intervals from 10 minutes to 1 hour. There exists a wide range of diagnostic models which have been used by scientists in problems of meteorology and air pollution.

The primitive 2-D diagnostic models did not consider the terrain orography and the vertical profile of the wind. They built an interpolated wind field taking into account only the distance from the nodes to the measurement stations and then they solved the two-dimensional elliptic problem arising from the discretization in a plane; see [16] for a 2-D adaptive finite element model with mixed formulation. Nowadays, in problems defined over complex terrain, to have high quality meshes is essential for the discretization of the studied domains. Most of the existing models uses to work with regular meshes. This strategy is impracticable for problems with complex terrain since the size of the elements must be very small in order to capture the digital information of the map. In this case, there would be regions with no fine details where such small element size would not be necessary. This would finally lead us to larger linear systems of equations and higher computational cost for solving them. Our first 3-D models (see [7, 18]) had some of these limitations since the meshes used for defining the terrain surface were regular. In [8], we presented a new finite element model that uses adaptive nonstructured meshes of tetrahedra with elements of small size where it is necessary but maintaining greater elements where such level of discretization is not required. The resulting 3-D mesh also contains more nodes near the terrain surface, where we need more precision. In a postprocess, the mesh is smoothed and, if necessary, untangled by using the Escobar et al algorithm [4] in

order to improve its quality. In addition, a local refinement procedure was proposed for improving the numerical solution [6]. Finally, although mass consistent models are widely used, they are often criticized because their results strongly depend on some governing parameters. This parameters are generally approximated using empirical criteria. Our model includes a tool for the parameter estimation based on genetic algorithms [8].

In order to check the model with realistic data, the company *Desarrollos Eólicos S.A.* (DESA) has provided us with technical support about digital terrain maps related to orography and roughness length, as well as measurements of wind and turbulence intensity in some anemometers located in Lugo (Spain). This work deals with the procedures required for inserting all of this information in the wind modelling. In section 2, we present the improvements to the surface mesh generation, including an adaptive procedure to capture the orography and roughness information simultaneously, additional local refinements in different regions of the terrain and a smoothing technique in order to improve the mesh quality and move edges on contour lines. The developed technique for inserting new information about wind measures at different heights and turbulence intensities is described in section 3. Section 4 is devoted to numerical experiments with examples that illustrate all the new possibilities of our wind model. Besides, a parameter estimation problem is solved using genetic algorithms for an episode along a day. Finally, we summarize the conclusions of this work and the topics that need further research.

2 Construction of the terrain surface mesh

Three improvements have been implemented in our mesh generation code. Orography and roughness length are two essential variables to be included in the wind model. If accurate information of the terrain orography and roughness is available, an adaptive procedure of mesh refinement/derefinement should be able to capture them simultaneously. These procedure has been carried out using two different derefinement parameters. In addition, sometimes we need more accuracy in the surrounding of the stations or any other control point on the terrain surface (e.g., in a wind farm). In such cases, the mesh must be refined around these points and, thus, a local mesh refinement has to be applied after the above procedure. Finally, in most applications there exist contour lines which define important properties of the terrain surface, e.g., the coast line, the roughness length contours, etc. In order to capture such lines with the mesh, a smoothing procedure has been developed. It is based on nodes movement, maintaining the mesh connectivities, such that a list of edges is superimposed on that lines as well as the triangulation quality is improved.

2.1 Mesh adaption to terrain orography and roughness length

The mesh generation process starts with the determination of nodes allocated on the terrain surface. Their distribution must be adapted to the orographic and roughness characteristics in order to minimize the number of required nodes. The procedure first builds a sequence of nested meshes $T = \{\tau_1 < \tau_2 < \ldots < \tau_m\}$ from a regular triangulation τ_1 of the rectangular region which is studied, such that the level τ_j is obtained by a global refinement of the previous level τ_{j-1} with the 4-T Rivara's algorithm [17]. Every triangle of level τ_{j-1} is divided into four subtriangles inserting a new node in the middle point of the edges and connecting the node inserted in the longer edge with the opposite vertex and with the other two new nodes. Thus, in the mesh level τ_j there appear new nodes, edges and triangles that are defined as corresponding to level j. The number of levels m of the sequence is determined by the degree of discretization of the terrain, i.e., the diameter of the triangulation τ_m must be of the order of the spacial step of the digital map that we are using (the spacial step of the roughness length map is often greater or equal to that of the orographic map). In this way, we ensure that this regular mesh is able to capture all the orographic and roughness information by an interpolation of the heights and roughness length in the nodes of the mesh. Finally, we define a new sequence $T' = \{\tau_1 < \tau'_2 < \ldots < \tau'_{m'}\}, m' \leq m$, applying the derefinement algorithm [19, 20]. In this step, two derefinement parameters ε_h and ε_r are introduced and they determine the accuracy of the approximation to the terrain surface and to its roughness length, respectively. The absolute difference between the height obtained in any point of the mesh $\tau'_{m'}$ and the corresponding exact height will be lower than ε_h. A similar condition is established for the roughness and ε_r. Finally, the derefinement algorithm (see algorithm 1) uses all the information of the element and edges genealogy defined in the sequence.

The derefinement condition takes into account both requirements of height and roughness simultaneously. On the one hand, we consider the analysis of the absolute difference between the exact height (usually referred to an interpolated value from the digital map) of a node and the interpolation of the height corresponding to the two extreme nodes of its environment edge, i.e., the edge in which that node was inserted in the middle point during the refinement process. On the other hand, the same analysis is carried out with the roughness length. If the first difference related to the height is lower than ε_h and the second difference related to the roughness length is lower than ε_r, simultaneously, then the node may be eliminated, although in some cases it will have to be kept due to conformity reasons.

We remark that the node connections of the resulting two-dimensional mesh may be modified when we construct the Delaunay triangulation in the three-dimensional domain [21], since what we need and keep is the location of its nodes. Also, the level to which each node belongs should be kept in order to generate the inner nodes in the domain [1, 2, 3].

Algorithm 1 Derefinement algorithm.

INPUT: Sequence $T = \{\tau_1 < \tau_2 < \ldots < \tau_m\}$.
for $j = m$ to 2 **do** {Loop in levels of T}
For each node corresponding to τ_j, the derefinement condition is evaluated and the nodes and edges that may be eliminated are marked by using derefinement vectors.
The conformity of the new mesh level j is ensured minimizing the derefined region.
if any node corresponding to τ_j stands **then**
New node connections are defined for the new level j: τ_j^j.
The vectors of the genealogy of τ_j^j and τ_{j-1} are modified.
else
The current level j is eliminated from the structure vectors.
The vectors of the genealogy of τ_{j-1} are modified.
end if
The changes in the mesh are inherited by the next meshes.
The structure vectors are compressed.
A new sequence of nested meshes T^j is obtained. This sequence is the input in the next step of the loop. $T^j = \{\tau_1 < \tau_2 < \ldots < \tau_{j-1} < \tau_j^j < \ldots < \tau_{m_j}^j\}$.
end for
OUTPUT: derefined Sequence $T' = T^2 = \{\tau_1 < \tau_2' < \ldots < \tau_{m'}'\}$.

2.2 Local refinement around control points

The resulting mesh adapted to orography and roughness is not always enough to ensure a prescribed accuracy of the numerical model in some regions of the domain and they may require a finner discretization. We have solve this problem by refining the terrain surface mesh in those regions such that the nodes inserted inside them are not eliminated after the derefinement procedure. The vertical spacing function and the 3-D Delaunay triangulation algorithm, that complete our 3-D mesh generator (see [1, 2, 3]), will produce a tetrahedral mesh refined around the selected regions. So, the user can define the form and location of these regions and the number of additional triangles subdivisions to be carried out inside them in order to obtain the required element size.

2.3 Surface mesh adaption to prescribed contours

Node movement provides a surface mesh the ability to match an arbitrary curve. Suppose that the surface mesh, M, is projectable on a unique plane P forming a parametric mesh, N. If C is a curve defined on P, our objective is to move some nodes of N, projecting them on C, to get an interpolation of C by edges of N. Note that, associated to this interpolation, there is a mapped interpolation on M. To achieve this objective we have to decide which nodes of N can be projected on C without inverting

any triangle of its local submesh. More accurately, we say that a free node q is projectable on C if it exists any point of C, say q', such that the resulting local submesh $N(q)$ has not any inverted triangle after carrying q to the position of q'. In general, if q is projectable, its possible placement on C is not unique and, therefore, we have to determine the "best" position to relocate q. To decide which is the best position of this node we could think on minimizing the objective function $\left|K_\eta^0\right|_n(\mathbf{x})$ [5] subject to the constrained $\mathbf{x} \in C$. Nevertheless, this function only works properly when $N(q)$ is not tangled. To overcome this problem we propose to modify this objective function following the criteria developed in [4]. This modification consists of substituting σ^0 by the positive and increasing function $h(\sigma^0)$, where σ^0 is a quantity appearing in the denominator of $\left|K_\eta^0\right|_n(\mathbf{x})$ that tends to zero as the area of the triangle does. In this way, the barrier associated with such singularities of $\left|K_\eta^0\right|_n(\mathbf{x})$ will be eliminated and the new function will be smooth all over $\mathbb{R}^2$. If $\left|K_\eta'^0\right|_n(\mathbf{x})$ is the modified objective function, the problem of finding the optimal position to project the free node on C is

$$\text{minimize } \left|K_\eta'^0\right|_n(\mathbf{x}),\ \text{subject to } \mathbf{x} \in C \tag{1}$$

The objective function $\left|K_\eta'^0\right|_n$ strongly penalizes the negative values of σ^0, so that, the minimization process of (1) leads to the construction of a local submesh $N(q)$ without inverted triangles, provided it is possible. Then, if $\bar{\mathbf{x}}$ is the minimizing position of (1) and $\sigma^0(\bar{\mathbf{x}}) > 0$ for all triangle of $N(q)$, we conclude that q is projectable on C and $\bar{\mathbf{x}}$ is its optimal position.

The projection of a free node on C can give rise to a local mesh with very poor quality. This effect is partly palliated after smoothing the remainder nodes, following the procedure described in [5]. Moreover, we have observed that the final mesh has better quality if the constraint $\sigma^0(\bar{\mathbf{x}}) > 0$ is substituted by the most restrictive one $\sigma^0(\bar{\mathbf{x}}) > \epsilon$ for all triangle of $N(q)$, were $\epsilon > 0$ is a decreasing parameter that tends to zero as the number of global iterations increases.

The nodes are inserted in the curve without specific criterion, just according to the increasing order of its numeration. This produces situations in which some sections of the curve C can not be interpolated by edges of the parametric mesh N.

In some applications we lack an analytic expression of the curve to be interpolated. Only a set of aligned points $\{q_c\}$, that approximately describes a contour, is available. This is the case, for example, of data supplied by digitalized maps describing shorelines, roughness contours, river banks, etc. To approach this situation we solve a discrete version of (1). Given local submesh $N(q)$, we analyze if q is projectable on any point of $\{q_c\}$, that is, we check if the condition $\sigma^0(\mathbf{x}) > \epsilon$ for all triangle of $N(q)$ is satisfied when $\mathbf{x}$ cover $\{q_c\}$. Among the positions $\mathbf{x}$ that satisfy previous condition we choose the optimal point, $\bar{\mathbf{x}}$, as the one that minimizes $\left|K_\eta'^0\right|_n$. We must underline that this problem is correctly defined only if the density of points of $\{q_c\}$ is high enough. Typically, the distance between contiguous points of $\{q_c\}$ must be much shorter than the distances between adjacent nodes of N.

Usually, most of nodes of N are very far from any point of $\{q_c\}$ and, therefore, they are not projectable, so it is advantageous to have a previous knowledge of which

nodes are candidates to be projected. A possibility is to associate to each node of both N and $\{q_c\}$ the square of a regular grid in which it is included. Let us suppose that the size of these squares is $d_{max} \times d_{max}$, being d_{max} the maximum edge present at the mesh. We can take a quick decision about if the node q is candidate to be projectable on $\{q_c\}$ only by inspecting the region, S_q, formed by the square that contains q and the surrounding squares. Firstly, we find the subset $\{q'_c\}$ of points belonging to $\{q_c\}$ and included in S_q. If $\{q'_c\} \neq \emptyset$, we analyze if q is projectable on $\{q'_c\}$ as it was explained above. Note that the distance between q and any point of the contour, outside S_q, is greater than d_{max} and, consequently outside the feasible region of $N(q)$ (the feasible region of $N(q)$ is included in the circle of radius d_{max} and center q).

3 Improvements to the wind model

Our wind model has been improved in order to consider the additional information that currently may be available at measurement stations. On the one hand, we have usually different stations located in the same tower for minimizing costs and fixing the wind profiles. Thus, the computation of the friction velocity, which was directly computed from a single wind velocity measured at a station, must be obtained from several measures. For this purpose, a least square approximation is carried out. On the other hand, these stations usually provides measures of the turbulence intensity which is related to the atmospheric stability of the region. So, the knowledge of the range of turbulence intensity will allow us to select the stability class. Following the Pasquill model for the atmospheric stability [22] and defining new ranges of turbulence intensity, a new table for Pasquill stability classification is built.

3.1 New computation of the friction velocity

We consider a log-linear profile [24] in the planetary boundary layer, which takes into account the horizontal interpolation [7], the effect of roughness length on the wind speed and direction, and the atmospheric stability (neutral, stable or unstable) following the Pasquill classification. In the surface layer a logarithmic wind profile is constructed,

$$\vec{v}_0(z) = \frac{\vec{v}^*}{k}\left(\ln\frac{z}{z_0} - \Phi_m\right) \qquad z_0 < z \leq z_{sl} \tag{2}$$

where $\vec{v}_0$ is the wind velocity, $k \simeq 0.4$ is the von Karman constant and z is the height of the considered point over the terrain level. The friction velocity $\vec{v}^*$ is obtained at each point from the interpolation of measures at the height of the stations (*horizontal interpolation*),

$$\vec{v}^* = \frac{k\ \vec{v}_0(z_e)}{\ln\frac{z_e}{z_0} - \Phi_m(z_e)} \tag{3}$$

Evidently, if n measures were available in a vertical line, the above equation would yield n different friction velocities,

$$\vec{v}_i^* = \frac{k\ \vec{v}_{0_i}(z_{e_i})}{\ln \frac{z_{e_i}}{z_0} - \Phi_m(z_{e_i})} \qquad i = 1, ..., n \tag{4}$$

In order to obtain the optimum value of $\vec{v}^*$, we solve a least square problem involving the wind velocities measured at different height and considering that the friction velocity is not a function of the height. Consider

$$A_i = \frac{1}{k}\left(\ln \frac{z_{e_i}}{z_0} - \Phi_m(z_{e_i})\right) \qquad i = 1, ..., n \tag{5}$$

such that

$$\vec{v}_{0_i}(z_{e_i}) = \vec{v}^* A_i \qquad i = 1, ..., n \tag{6}$$

Then, the function to be minimized is,

$$F_{obj} = \sum_{i=1}^{n} \left(\vec{v}_{0_i}(z_{e_i}) - \vec{v}_{s_i}(z_{e_i})\right)^2 = \sum_{i=1}^{n} \left(\vec{v}^* A_i - \vec{v}_{s_i}(z_{e_i})\right)^2 \tag{7}$$

whose minimum is obtained for the following friction velocity,

$$\vec{v}^* = \frac{\sum_{i=1}^{n} A_i \vec{v}_{s_i}(z_{e_i})}{\sum_{i=1}^{n} A_i^2} \tag{8}$$

3.2 Atmospheric stability versus turbulence intensity

The atmospheric stability is related to the atmospheric turbulence as well as to the vertical gradient of temperature and situations of thermal inversion. It provides a qualitative measure of the air density variations due to changes of pressure and temperature which affect to some atmospheric motions. The atmospheric conditions may be classified as stable, unstable or neutral. Under stable conditions, if a mass of air blows up, it will find warmer air around what will make it go down. On the contrary, if it blows down, it will find colder air around and it will attempt to go up. This tendency of the air to stand in the same layer is called stability of the atmospheric stratification. For unstable conditions the potential temperature decreases with the height and the vertical motion augments, i.e., if the air goes up it will find colder air which will make it go up. However, if it go down it will find warmer and light air, and it will go on falling. Finally, if a volume of air (after a vertical motion in an atmospheric layer without mixing with the surrounding air) experiments a null net vertical force, the motions will not be affected by the thermal gradient and the atmospheric layer is assumed to be neutral. Under these conditions, such volume does not try to get back to its original position (stable stratification) nor accelerate and go far from it (unstable stratification).

The atmospheric stability may be characterized by using the Pasquill stability classification of table (1). It considers the following classes for stability: A (extremely unstable), B (moderately unstable), C (slightly unstable), D (neutral), E (slightly stable) and F (moderately stable) [22].

Pasquill stability class

	Isolation			Nighttime	
Surface wind speed (m/s)	Strong	Moderate	Slight	$\geq 4/8$ Clouds	$\leq 3/8$ Clouds
< 2	A	A-B	B	-	-
$2-3$	A-B	B	C	E	F
$3-5$	B	B-C	C	D	E
$5-6$	C	C-D	D	D	D
> 6	C	D	D	D	D
For A-B, take the average of the values of A and B, etc.					

Table 1: Pasquill Stability Classification depending on the surface wind speed and the isolation. Strong isolation corresponds to a sunny afternoon of the middle-summer in England; slight isolation is related to same conditions in middle-winter. Nighttime means the time from one hour before the sunset to one hour after the sun rises. Neutral class D should be used also, independently of the wind speed, for clouded sky along the day or the night, and for any condition of the sky during the hour before and after the nighttime.

The anemometers generally provides measures of the intensity of turbulence that may help to complete the information about the class of atmospheric stability in the studied region. The intensity of turbulence i is defined as the square root of the sum of variances $\sigma_u^2,\ \sigma_v^2,\ \sigma_w^2$, of the three components of the velocity $u_0,\ v_0,\ w_0$, respectively, divided by the average wind velocity that has been measured,

$$i = \frac{\sqrt{\sigma_u^2 + \sigma_v^2 + \sigma_w^2}}{|\vec{v}_0|} \tag{9}$$

However, only measures of speed variations are often available but not of the wind direction. In such cases, equation (9) is reduced to,

$$i = \frac{\sigma_{v_0}}{|\vec{v}_0|} \tag{10}$$

where σ_{v_0} represents the standard deviation of the measured wind speeds.

While an unstable atmosphere implies a high level of turbulence, with a range of turbulence intensities between 0.2 and 0.4 approximately, a stable atmosphere, with a small or almost null turbulence, is characterized by intensities from 0.05 to 0.1 [23]. In table 2, the above relations of the turbulence intensity and the atmospheric stability have been considered in order to define the Pasquill stability class.

Pasquill stability class							
	Isolation				Nighttime		
Surface wind speed (m/s)	$i > 0.35$	$0.35 \geq i > 0.25$	$0.25 \geq i > 0.15$	$0.15 \geq i$	$i > 0.075$	$0.075 \geq i > 0.03$	$0.03 \geq i$
$\|v_0\| < 2$	A	B	B	B	F	F	F
$2 \leq \|v_0\| < 3$	A	B	C	C	E	E	F
$3 \leq \|v_0\| < 5$	B	B	C	C	D	E	E
$\|v_0\| \geq 5$	C	C	C	D	D	D	D

Table 2: Pasquill stability classification taking into account the surface wind speed and the turbulence stability.

4 Numerical experiments

We have selected some test problems in order to show the improvements carried out in our wind model. The first illustrates the capability of the mesh generator for adapting to the main characteristics of the terrain corresponding to the studied domain. Next experiments are related to the surface mesh adaption to any prescribed contour. Finally, we present a realistic modelling of a wind episode along a day, including the estimation of the parameters that govern the model, the wind modeling and a comparison with available data of wind in control points. All experiment were run on a XEON precision 530, except the parameter estimation problem which was solved using a cluster of PCs.

4.1 Surface mesh adaption to orography and roughness

The studied three-dimensional domain is located in a region of Lugo, Spain, at $43N$ of latitude and it is defined by four points of UTM coordinates $A(609980,\ 4799020)$, $B(626000,\ 4799020)$, $C(626000,\ 4813040)$ and $D(609980,\ 4813040)$, respectively. The height of the top is $4000\ m$. A digital topographic map was provided by *DESA* on a mesh of element size $20 \times 20\ m$. The X axis corresponds to East direction and the Y one to North. Thus, we are working with a region of $16020 \times 14020\ m$. The minimum and maximum heights are $420\ m$ and $1020\ m$, respectively. Figure 1 represents the heights of the terrain. The measurement stations and the control points has been approximately plotted, such that from North to South we can find E243, E208, E212, E242, E206 and E283. Roughness is an essential factor on the atmospheric stratification, and therefore, on the characteristics of the resulting wind profile. Figure 2 shows the roughness length of the terrain which were supplied by *DESA*. We remark that some stations and control points are closed to contours of the roughness. In this case, the roughness length values are $0.03\ m$, $0.05\ m$, $0.08\ m$, $0.3\ m$ and $0.8\ m$.

Starting from a regular mesh of the rectangular region with element size of $1 \times 1\ km$

Station	UTM-E	UTM-N	Height
E206	615396	4805218	924.8
E208	616917	4807256	945.0
E212	617423	4806382	895.0

Table 3: Coordinates in m of the measurement stations.

Control point	UTM-E	UTM-N	Height
E242	618290	4806136	873.2
E243	616629	4808235	947.0
E283	617473	4804111	849.0

Table 4: Coordinates in m of the control points.

approximately, five global refinements are carried out using 4-T Rivara's algorithm [17]. With this number of refinement steps, we obtain a mesh with an element size about $31\ m$. In order to improve the discretization near the stations and control points, five additional local refinements are applied inside six circles with centre at the stations and control points, respectively, and diameter $200\ m$. This produces a local element size about $1\ m$. Once we have interpolated the height and the roughness length in the nodes of these refined two-dimensional mesh, we use the derefinement algorithm [19, 20] described in section 2.1 with $\varepsilon_h = 10$ and $\varepsilon_r = 0.01$, keeping in any case the nodes located inside the circles. In figure 3 we can see the resulting triangulation of the terrain surface. The corresponding three-dimensional mesh contains 102662 nodes and 515812 tetrahedra.

4.2 Surface mesh adaption to prescribed contours

In many cases of environmental modelling, there are some contour lines which determinate certain characteristics of the studied region. For example, in wind simulation the well definition of shore lines or roughness contours may be very important for obtaining accurate results. Thus the mesh must be adapted following these contours such that they are represented by edges of the mesh. Figure 5 shows the adaption of the initial mesh of figure 4, related to a region of the north west of Gran Canaria Island, to the shore line (plotted by points in red). The second example corresponds to a mesh of another region of Gran Canaria Island in the surrounding of the Arucas Mountain (figure 6) that is adapted to a spiral around the mountain (figure 7). In this view, we can clearly see how the edges of the mesh end up being placed on the curve. Although we have chosen these 2-D representations, we remark that both examples are meshes constructed over 3-D surfaces.

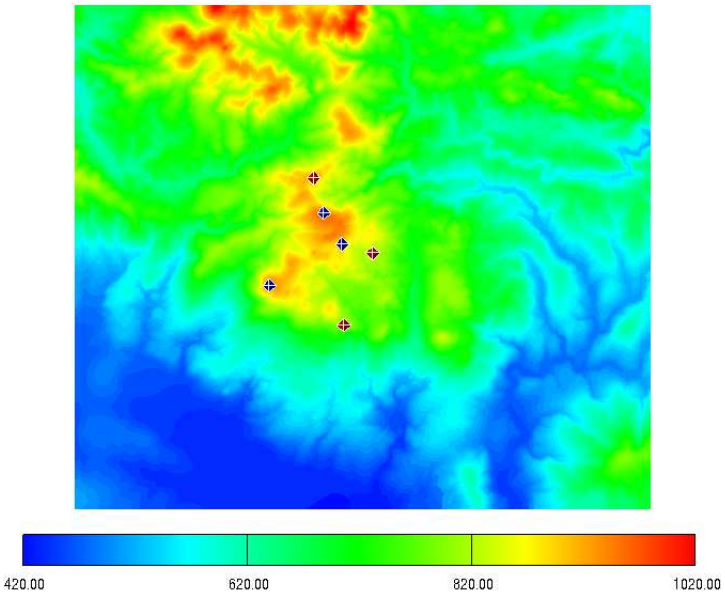

Figure 1: Topographic map of the studied region in Lugo. From North to South, we can see the stations or control points E243, E208, E212, E242, E206 and E283.

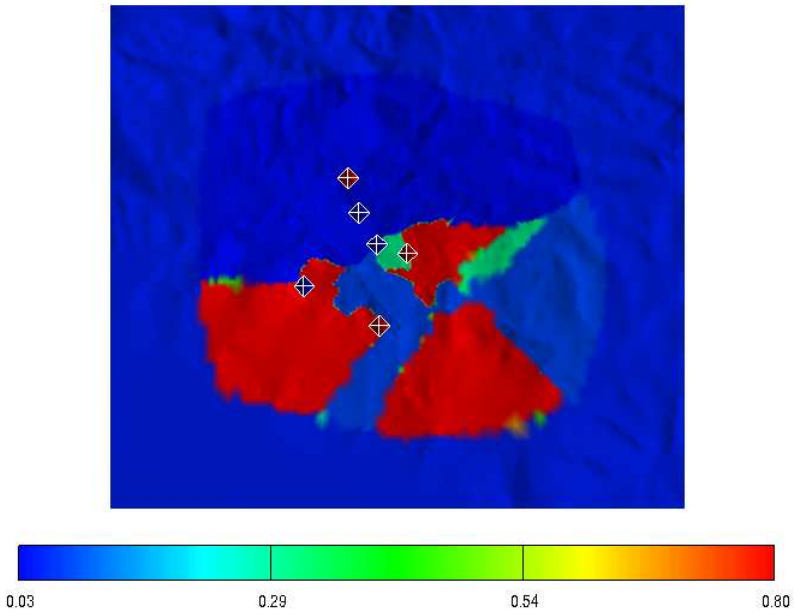

Figure 2: Roughness length map of the studied region in Lugo with the station and control points.

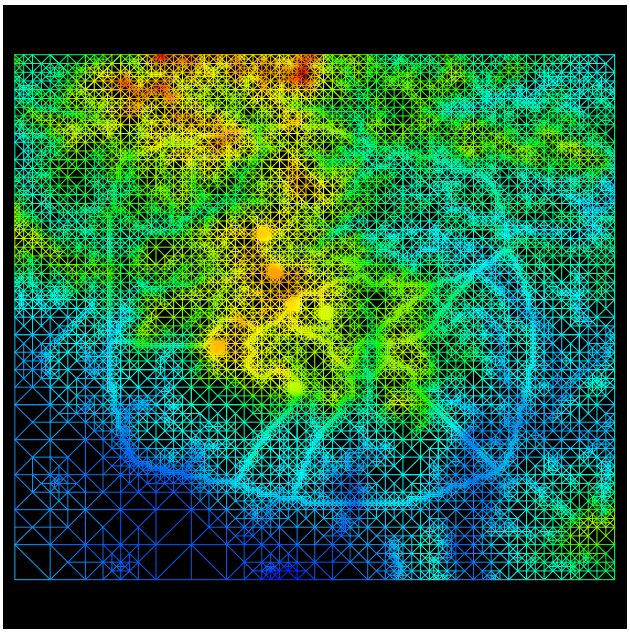

Figure 3: Mesh adapted to the orography and roughness of the terrain corresponding to the studied region in Lugo.

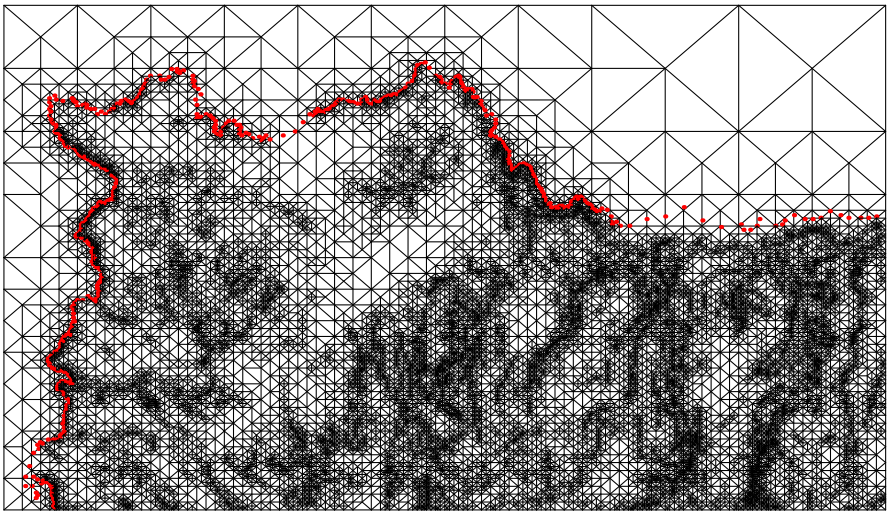

Figure 4: Region defined in the north west of Gran Canaria Island. Contour plots and initial mesh to be adapted.

4.3 Wind simulation in a realistic episode

Using the mesh constructed for the Lugo application in the first numerical experiment, we have made a simulation for an episode along the March 21, 2003. The first step is to estimate the main parameters of the model and, then, apply the wind model using

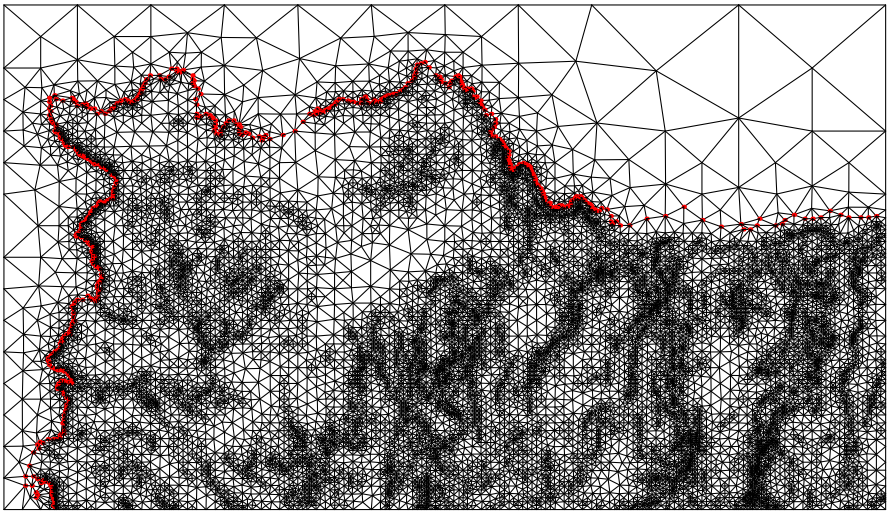

Figure 5: Region defined in the north west of Gran Canaria Island. Contour plots and adapted mesh.

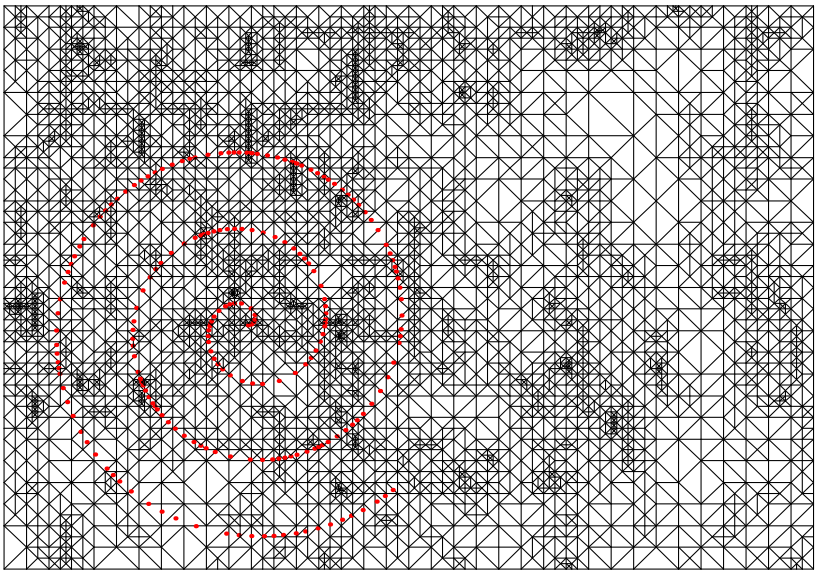

Figure 6: Region defined in the surrounding of Arucas Mountain (Gran Canaria Island). Contour is defined as an spiral line around the mountain to which the initial mesh must be adapted.

the estimated values. Next, the wind velocity is checked in the control points, where the wind data is supplied by *DESA*.

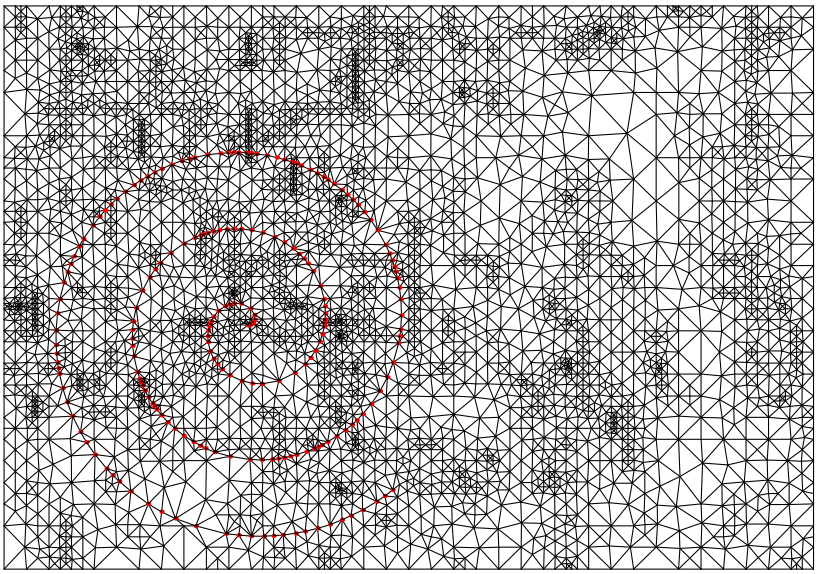

Figure 7: Region defined in the surrounding of Arucas Mountain. Contour plots and adapted mesh.

4.3.1 Parameter estimation along a day

We have taken into account the table 2 for determining the stability class from the available turbulence intensity values. For the studied day, we have obtained neutral conditions. So we must estimate the stability parameter α, the weighting parameter ε related to the horizontal interpolation of wind velocities and the parameter γ involved in the computation of the planetary boundary layer; see, e.g., [8]. The estimation has been carried out each hour (24 computations). We has applied genetic algorithms to solve these parameter estimation problems, where the fitness functions are defined in terms of the relative velocity errors obtained by the model at the measurements stations. In figure 8 we can see the evolution of the values of the three parameters along the episode. The values of ε are practically constant and approximately equal to 1. This means that only the horizontal distance has effect on the horizontal interpolation. This result is agreed with the orographic characteristics of the studied domain. Likewise the values obtained for γ are closed to 0.15, that is, the lower limit for this parameter which is related to low planetary boundary layers. However, the stability parameter α varies in the interval 8-20. This range of values makes the wind predominantly flow more over the obstacles than around them.

4.3.2 Comparison of the model results with empirical data

Once the main parameters are estimated, we start the wind modelling along the selected episode using the obtained values. As example, we show the wind map of the

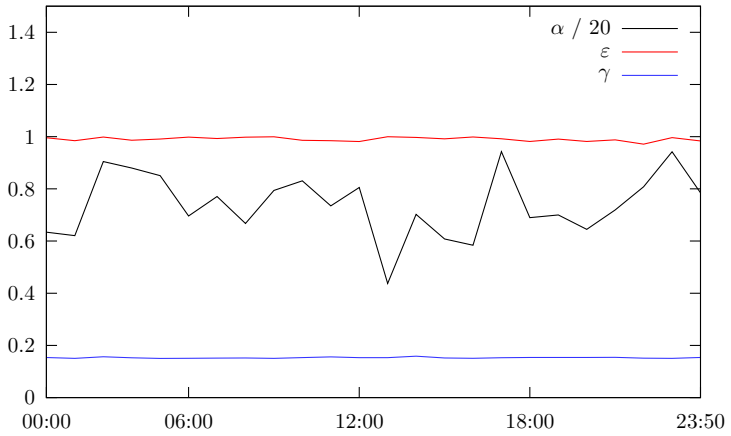

Figure 8: Results of the estimation of α, ε and γ along the studied episode (March 21, 2003)

region at 12:00 hours of March 21, 2003. Figure 9 represents the speed of wind at $40\ m$ over the terrain. For the studied day, only measures from E242 and E283 were available. Figures 10 and 11 show the wind speeds obtained with the model and the reference values measured at the control points E242 and E283, respectively. More details of the errors of computed winds with respect to the measured wind may be seen in table 5. We remark that the average errors at the measurement stations are small as expected. The average error is 27.24% at control point E242 and 4.94% at E283.

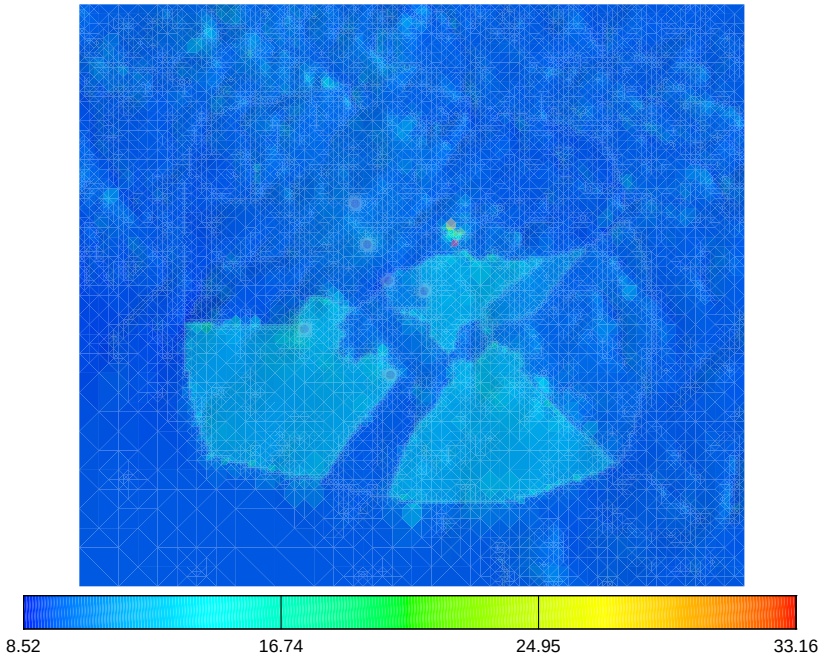

Figure 9: Wind map relative to the region of Lugo at 12:00 of March 21, 2003.

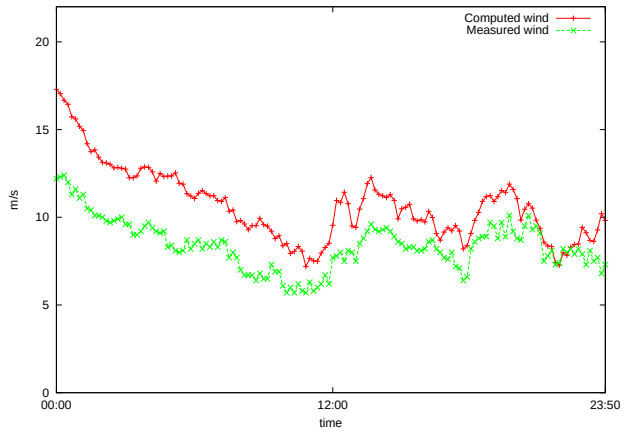

Figure 10: Comparison of the wind velocities measured at the control station E242 (March 21, 2003).

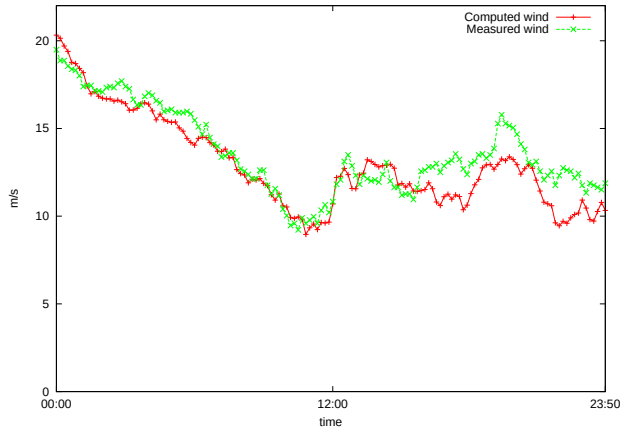

Figure 11: Comparison of the wind velocities measured at the control station E283 (March 21, 2003).

Stations and control points	Average measured wind	Average computed wind	% average error	Maximum absolute error	Minimum absolute error
E206 ($49\ m$)	15.37	15.50	0.81 %	0.46	0.01
E208 ($15\ m$)	8.57	8.98	4.74 %	1.25	0.00
E208 ($30\ m$)	9.25	9.92	7.21 %	1.36	0.05
E212 ($15\ m$)	8.46	8.44	0.20 %	0.63	0.00
E212 ($30\ m$)	9.02	9.85	9.25 %	1.60	0.31
E242 ($40\ m$)	8.40	10.69	27.24%	5.09	0.09
E283 ($49\ m$)	13.62	12.95	4.94 %	3.04	0.02

Table 5: Error of the computed wind at stations and control points.

5 Conclusions

We have proposed a technique for constructing tetrahedral meshes which are simultaneously adapted to the terrain orography and the roughness length. The use of our refinement/derefinement process in the 2-D mesh corresponding to the terrain surface allows us to obtain meshes that are accurately adapted to different functions as well as are locally refined around several points. These characteristics of the generated meshes are very important in the wind simulation since, on the one hand, the quality of the representation of both orography and roughness is critical for obtaining accurate results with the model, and on the other hand, the local refinement at the stations and control points is essential for inserting the wind data of the stations or recovering such data at any required point.

Some improvements have been carried out in the construction of the initial wind based on the horizontal interpolation of wind measures and vertical extrapolation in stratified atmosphere. The optimization of the friction velocity for several measures in the same tower allows to minimize the differences between the constructed vertical profile of wind and the measures. However, though such differences are small, further research is needed in order to construct new wind profiles that exactly satisfy all the available measures of wind velocities. In addition, the inclusion of observations of turbulence intensities has made the model to be able of automatically updating the suitable wind profile as function of the corresponding stability class.

The periodic updating of the main parameters of the model has proved to be fundamental for reducing the errors of the computed wind. However, further considerations should be taken into account in future works for a better performance of the model. For example, a finer map of roughness, a more sophisticated horizontal interpolation of wind velocities and a greater number of measurement stations well distributed over the studied region, will help to reduce errors at points like E242 where the roughness may not be well approximated. Finally, in order to obtain an accurate wind field in zones with very steep slopes, the mesh should be adapted to the contour lines, since a change in the direction of edges in the mesh may strongly affect the computed wind.

Acknowledgement

The work has been partially supported by the Spanish Government (Ministerio de Educación y Ciencia) and FEDER, grant number CGL2004-06171-C03-02/CLI. The authors are also grateful to Ignacio Láinez and Antonio Ruiz from *Desarrollos Eólicos S.A.* for their technical support and the wind data corresponding to their wind farm in Lugo.

References

[1] Montenegro R, Montero G, Escobar JM, Rodríguez E, González- Yuste JM. Tetrahedral Mesh Generation for Environmental Problems over Complex Terrain. Lect Notes Comp Sci 2002;2329:335-44.

[2] Montenegro R, Montero G, Escobar JM, Rodríguez E. Efficient Strategies for Adaptive 3-D Mesh Generation over Complex Orography. Neural, Par Sci Comput 2002;10:57-76.

[3] Montero G, Montenegro R, Escobar JM, Rodríguez. Generación automática de mallas de tetraedros adaptadas a orografías irregulares. Rev Int Mét Num Cálc Dis Ing 2003;19(2):127-44.

[4] Escobar JM, Rodríguez E, Montenegro R, Montero G, González-Yuste JM. Simultaneous untangling and smoothing of tetrahedral meshes. Comput Methods Appl Mech Engrg 2003;192:277587

[5] Escobar JM, Montero G, Montenegro R, Rodríguez E. An Algebraic Method for Smoothing Surface Triangulations on a Local Parametric Space. Int. J. Numer. Meth. Engrg. In press.

[6] González-Yuste JM, Montenegro R, Escobar JM, Montero G, Rodríguez E. Local Refinement of 3-D Triangulations Using Object-Oriented Methods. Adv Engrg Soft 2004;35:693-702.

[7] Montero G, Montenegro R, Escobar JM. A 3-D Diagnostic Model for Wind Field Adjustment. J Wind Engrg Ind Aer 1998;74-76:249-61.

[8] Montero G, Rodríguez E., Montenegro R, Escobar JM, González- Yuste JM. Genetic Algorithms for an Improved Parameter Estimation with Local Refinenent of Tetrahedral Meshes in a Wind Model. Adv Engrg Soft 2005;36:3-10.

[9] Michalewicz Z, Genetic Algorithms + Data Structures = Evolution Problems. Springer Verlag, Berlin-Heidelberg-New York, 1994.

[10] Rodríguez E, Montero G, Montenegro R, Escobar JM, González- Yuste JM. Parameter Estimation in a Three-dimensional Wind Field Model Using Genetic Algorithms. Lect Notes in Comp Sci 2002;2329:950-9.

[11] Pielke, R. Mesoscale Meteorological Modeling. Academic Press, Inc., Orlando, Florida, 1984.

[12] Lalas DP, Tombrou M, Petrakis M. Comparison of the Performance of Some Numerical Wind Energy Siting Codes in Rough Terrain. European Community Wind Energy Conference, Herning, Denmark, 1988.

[13] Pennel, WT. An Evaluation of the Role of Numerical Wind Field Models in Wind Turbine Siting. Batelle Memorial Institute, Pacific Northwest Laboratory, Richland, Washington, 1983.

[14] Kitada T,Kaki A, Ueda H, Peters LK. Estimation of Vertical Air Motion from Limited Horizontal Wind Data - A Numerical Experiment. Atmos Environ 1983;17:2181-2192.

[15] Moussiopoulos N, Flassak Th, Knittel G. A Refined Diagnostic Wind Model. Environ. Software 1988;3:85-94.

[16] Winter G, Montero G, Ferragut L, Montenegro R. Adaptive Strategies Using Standard and Mixed Finite Elements for Wind Field Adjustment. Solar Energy 1995;54(1):49-56.

[17] Rivara, MC. A Grid Generator Based on 4-Triangles Conforming. Mesh-Refinement Algorithms. Int J Num Meth Engrg 1987;24:1343-1354.

[18] Montero G, Sanin N. Modelling of wind field adjustment using finite differences in a terrain conformal coordinate system. J Wind Engrg Ind Aer 2001;89:471-488.

[19] Ferragut L, Montenegro R, Plaza A. Efficient refinement/derefinement algorithm of nested meshes to solve evolution problems. Comm Num Meth Engrg 1994;10:403-12.

[20] Plaza A, Montenegro R, Ferragut L. An improved derefinement algorithm of nested meshes. Advances in Engineering Software 1996;27(1/2):51-7.

[21] Escobar JM, Montenegro R. Several aspects of three-dimensional Delaunay triangulation. Advances in Engineering Software 1996;27(1/2):27-39.

[22] Seinfeld JH, Pandis SN. Atmospheric Chemistry and Physics. From Air Pollution to Climate Change. John Wiley & Sons, Inc., New York, 1998.

[23] Mikkelsen T. Modelling of pollutant transport in the atmosphere. MANHAZ position paper, Risø National Laboratory, Denmark, 2003.

[24] Lalas DP, Ratto CF. Modelling of Atmospheric Flow Fields. World Scientific Publishing, Singapore, 1996.